

DETC2004-57476

MANIPULABILITY-BASED CONFIGURATION EVALUATION OF COOPERATIVE PAYLOAD TRANSPORT BY MOBILE ROBOT COLLECTIVES

Chin Pei Tang

Mechanical and Aerospace Engineering
State University of New York at Buffalo
318 Jarvis Hall, Buffalo NY 14260
E-mail: chintang@eng.buffalo.edu
Web: <http://www.eng.buffalo.edu/~chintang>

Venkat Krovi

Mechanical and Aerospace Engineering
State University of New York at Buffalo
318 Jarvis Hall, Buffalo NY 14260
E-mail: vkrovi@eng.buffalo.edu
Web: <http://www.eng.buffalo.edu/~vkrovi>

ABSTRACT

Interest in cooperative systems typically arises when certain tasks are either too complex to be performed by a single agent or when there are distinct benefits that accrue by cooperation of many simple agents. A quantitative examination of performance enhancement, due to the implementation of cooperation, is critical. In this paper, we focus on the development of a quantitative performance-analysis framework for a cooperative system with multiple wheeled mobile manipulators physically transporting a common payload.

Each mobile manipulator module consists of a differentially-driven wheeled mobile robot with a mounted planar three-degree-of-freedom (d.o.f.) manipulator. A composite cooperative system is formed when a payload is placed at the end-effectors of multiple such modules. Such a system possesses the ability to change its relative configuration as well as accommodate relative positioning errors of the mobile bases. However, the combination of nonholonomic constraints due to the mobile bases, holonomic constraints due to the closed kinematic loops formed and the varying actuation of the joints within the cooperative system requires careful treatment for realizing the payload transport task.

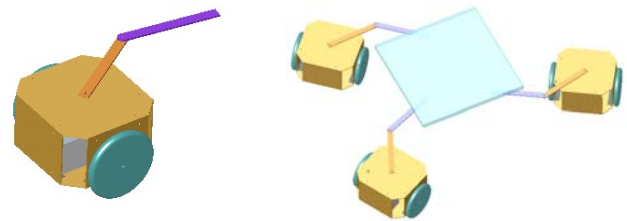
In this paper, we will analyze the cooperative composite system within a constrained mechanical system framework, by extending methods developed for treatment of articulated-closed-chain systems. Specifically, we will focus on the velocity-level kinematic modeling, while taking into account the nonholonomic/holonomic constraints and different joint-actuation schemes within the system. We then examine the applicability of a manipulability measure (isotropy index), to quantitatively analyze the system-level performance of the cooperative system, with these different joint-actuation schemes, with representative case-studies.

KEYWORDS

Cooperative robot collectives, mobile manipulator agents, nonholonomic/holonomic constraints, varied joint actuation, manipulability-based performance measures.

INTRODUCTION

Our overall goal is the design, analysis and implementation of a flexible, scalable system of multiple wheeled-mobile agents, that are individually autonomous but can team up to cooperatively transport large objects. Such frameworks for remotely controlled or remotely supervised cooperation of multiple autonomous mobile robots have applications for material handling tasks in many fields [1]-[3].



(a) (b)
Figure 1: (a) Representative mobile manipulator module and (b) representative composite formation of cooperative system

In our design, the individual autonomous agents take the form of differentially-driven wheeled mobile manipulators, consisting of an articulated arm attached to a mobile base. Each mobile base possesses a single rigid axle between two fixed disk wheels and the usual complement of nonholonomic kinematic constraints. The attached articulated-arm permits relative planar motion of the end-effector w.r.t the base platform in the horizontal plane. Various types of articulated

arms have been examined for suitability for the proposed cooperative payload transport task (see [3] for more details.) For this paper, we will assume that the articulated arm has *three* revolute joints – forming the so-called Type I mobile manipulator [3] – as shown in Figure 1(a).

A composite multi-degree-of-freedom (MDOF) system is formed when a common payload is placed on the end-effector of the two or more adjacent modules, as shown in Figure 1(b). The attached arms act like a compliant suspension system, which with suitable instrumentation and actuation endows the composite system with: (i) ability to accommodate changes in the relative configuration; (ii) redundant sensing for localizing the modules; and (iii) redundant actuation for moving the common payload while compensating for environmental disturbances and errors.

In particular, these articulations (with at least 3 d.o.f) permit the relaxation of the requirement for a common "Center of Rotation" between the multiple axles created by the *nonholonomic constraints* at the wheels. However, while the velocity-level kinematic constraints for the system are eliminated, other holonomic constraints (due to the closed kinematic loops) are introduced between the relative motions of the bases. Such *closed kinematic loops* present a number of subtleties that are not often seen in open kinematic chain manipulators. Notably, the kinematic configuration space of a closed loop manipulator is no longer a flat space but becomes a curved manifold embedded in a higher dimensional vector space. Further, as we can see in the major discussion in this paper, the existence of the holonomic (loop-closure) constraints, limit the d.o.f and hence not all articulations need to be actuated. Thus, the selection of the *location of the active and passive joints* also plays a vital role in determining the overall performance of the system.

In this paper, we will analyze the cooperative composite system within a constrained mechanical system framework. Specifically, we will focus on the kinematic modeling while taking into account (a) the nonholonomic constraints due to the wheel assemblies together with the holonomic constraints due to the kinematic closed-loops, and (b) varying location and actuation of the joints within the system. Performance of several cooperative system scenarios with varying actuation arrangements are then quantified in terms of the system-level manipulability measure.

The rest of the paper is organized as follows: Section II presents a brief overview of the pertinent literature followed by an overview of the adopted mathematical background in Section III. The kinematic model of the wheeled mobile manipulator module is introduced in Section IV. This is then used in Section V to model the composite-system with kinematic closed-loop constraints and formulate system-level manipulability-based measures-of-performance. Different case studies of cooperative payload transport, with varying actuation schema, are examined in terms of these system-level manipulability-based measures in Section VI. A brief discussion and concluding remarks are presented in Section VII.

II. LITERATURE SURVEY

Cooperative multi-robot systems, ranging from multiple mobile robots [4],[5], multiple manipulators [6], multi-fingered hands [7],[8] and multi-legged vehicles [9][10] have been extensively studied in a variety of contexts. We will restrict our attention to

cooperative physical manipulation by articulated mechanical systems focusing on the motion distribution issues.

Cooperating Articulated Mechanical Systems: The characteristic feature of such systems is the formation of closed kinematic chains, typically with one reference member interacting with a number of supporting serial chains. The nature of the attachment of the supporting chains to the reference member permits a *structural classification* [11] into *Type 0* systems, (such as multi-arm systems and dextrous hands) and *Type 1* systems (such as legged machines). At the same time, the presence of these closed kinematic chains reduces the effective degrees of freedom of the system, creating kinematic redundancy and most often redundancy in actuation [9]. This permits an alternate *functional classification* into *underactuated*, *exactly-actuated* and *redundantly-actuated systems*.

Cooperating System of Mobile Manipulators: However, there is relatively less literature, but considerably greater variability, in the approaches employed for cooperation of multiple mobile manipulators [12]-[16]. Khatib et al. [11] developed a decentralized control structure for cooperative tasks with mobile manipulation systems with *holonomic bases* and *fully actuated* manipulators. Motion planning has also been considered for collaborating teams of nonholonomic mobile manipulators from various centralized perspectives [13],[14]. Kuge et al. [15] propose a simple method for carrying a large object by cooperation of multiple mobile manipulators with *impedance based controllers* by *selectively locking and unlocking* some joints of the mounted manipulators on mobile platforms. Yamakita et al. [16] implement the Passive Velocity Field Control approach for the cooperative control of multiple mobile robots holding an object. However, in most cases, the focus is on a fully actuated manipulator, without the possibility of including any passive or semi-passive joints, which is a significant feature in our system.

The composite system formed by connecting the multiple mobile manipulators to the common payload also forms a subclass of the larger class of Multi-Degree-of-Freedom (MDOF) Wheeled Vehicles [17]- [23]. While some of these like the RollerRacer [17] and the Snakeboard [18] are case-studies in underactuated locomotion, several others like OMNIMATE/CLAPPER [19] and systems with multiple actively steered wheels [20]-[22] and WAAVs [23] feature redundancy in actuation. Several of these authors also note that despite gains in maneuverability over conventional mobile robots, the overconstrained nature with hybrid series-parallel kinematic chains creates challenges in planning and control of such wheeled systems.

Performance Measures: *Performance measures* play a critical role in design, evaluation, optimization and control of robotic systems. Performance measures for a individual robotic system are very well developed, including several Jacobian-Based Performance Measures (JBPM), such as manipulability, singularity and dexterity [24].

However, the literature on extension of such performance measures to groups of robots is relatively limited. Traditionally, variances in robots within a team were classified only as heterogeneous or homogeneous. Balch [25] developed a quantity called the social entropy to provide a quantitative evaluation of diversity and information level cooperation in robot teams. Alternatively, energy-based measures [26],[27],

developed from left-invariant Riemannian metrics [28] have been used to characterize the total kinetic energy of a collective at any instant of time, or over the entire maneuver.

While these measures show considerable promise, in this paper, we will focus our attention solely on Jacobian-based manipulability measures to serve as measure of motion and force transmission capability. Building from Yoshikawa's measure of manipulability [29] for the serial-chain case, a large variety of manipulability-based formulations have been used in different applications [8],[30]-[31]. The use of Singular Value Decomposition (SVD) of the Jacobian matrix offers further mathematical and geometrical insight of the manipulability characteristics of a robotic system [24]. Efforts for characterizing the manipulability of parallel-chain mechanisms [32]-[34] have noted the engendered difficulties. Such systems possess multiple closed kinematic loops whose loop closure constraints are responsible for considerable kinematic (and often actuation) redundancy within the system. Further, even in non-redundant settings, selection of the location of active/passive joints can significantly affect the manipulability, which we will explore in this paper. We will adapt some aspects of the existing work [32]-[34], extending it to include nonholonomic constraints within the formulation to facilitate performance evaluation of our composite system.

III. MATHEMATICAL BACKGROUND

In this section, we will briefly summarize the mathematical preliminaries required for the formulation, and the reader is referred to [35] for greater detail.

The configuration of a moving frame $\{E\}$ relative to a fixed frame $\{F\}$ can be defined in the planar Euclidean task space, $SE(2)$, by the homogeneous transformation:

$${}^F A_E = ({}^F R_E, {}^F \underline{d}) = \begin{bmatrix} {}^F R_E & {}^F \underline{d} \\ 0 & 0 & 1 \end{bmatrix} \quad (1)$$

where ${}^F R_E$ is a 2×2 rotation matrix of frame $\{E\}$ with respect to frame $\{F\}$, and ${}^F \underline{d}$ is a 2×1 displacement vector from the origin of frame $\{F\}$ to the origin of frame $\{E\}$. A *body-fixed* twist matrix corresponding to the motion of the moving frame $\{E\}$ with respect to its immediately preceding frame $\{F\}$ (as expressed in the moving frame $\{E\}$) is given by

$${}^E [{}^F T_E] = [{}^F A_E]^{-1} \left[\frac{d}{dt} [{}^F A_E] \right] = \begin{bmatrix} {}^E [{}^F \Omega_E] & {}^E [{}^F \underline{v}_E] \\ 0 & 0 & 0 \end{bmatrix} \quad (2)$$

where ${}^E [{}^F \Omega_E] = \begin{bmatrix} 0 & -\omega_z \\ \omega_z & 0 \end{bmatrix}$ and ${}^E [{}^F \underline{v}_E] = [v_x \ v_y]^T$. The

twist matrix ${}^E [{}^F T_E]$ can also be reassembled as a 3×1 twist vector as

$${}^E [{}^F \underline{t}_E]^T = [\omega_z \ \underline{v}^T] \quad (3)$$

Note that $\underline{v} = (v_x, v_y)$ and ω_z are the instantaneous linear and angular velocities of frame $\{E\}$ with respect to frame

$\{F\}$ (as expressed in the moving frame $\{E\}$). We note that the overall motion description in a body-fixed frame is useful for the study of locomotion systems, due to the engendered invariances to changes of the inertial frame $\{F\}$. Such a twist matrix can then be transformed to any arbitrary frame $\{N\}$ by a similarity transformation

$${}^N [{}^F T_E] = [{}^N A_E] {}^E [{}^F T_E] [{}^N A_E]^{-1} \quad (4)$$

The total twist at the end-effector of a serial-chain may be expressed as the linear combination of twist contributions of individual articulations in the chain, expressed in a common frame. For instance:

$${}^E [{}^F T_E] = \underbrace{[{}^E A_1]^{-1} [{}^1 T_E] [{}^E A_1]}_{\underline{t}_1} + \underbrace{[{}^E A_2]^{-2} [{}^2 T_E] [{}^E A_2]^{-1}}_{\underline{t}_2} + \dots + \underbrace{[{}^E A_N]^{-1}}_{\underline{t}_N} \quad (5)$$

These twist matrices can also be rewritten as linear combinations of twist vectors parameterized by the corresponding manipulation rates $\underline{v} = [v_1 \ v_2 \ \dots \ v_N]^T$. A geometrically assembled Jacobian matrix (J) may now be written as

$${}^E [{}^F \underline{t}_E] = \underbrace{\begin{bmatrix} \underline{t}_1 & \underline{t}_2 & \dots & \underline{t}_N \end{bmatrix}}_J \begin{bmatrix} v_1 \\ v_2 \\ \vdots \\ v_N \end{bmatrix} \quad (6)$$

where $\underline{t}_1, \underline{t}_2, \dots, \underline{t}_N$ are the twist vectors corresponding to the manipulation rates of v_1, v_2, \dots, v_N , respectively.

IV. KINEMATIC MODEL OF INDIVIDUAL MOBILE MANIPULATOR MODULE

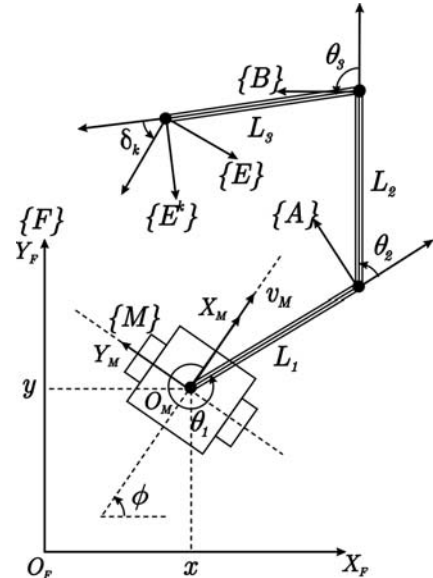


Figure 2: Kinematic model of individual wheeled mobile manipulator module

We consider a mobile manipulator with a differentially-driven wheeled mobile robot (WMR) platform and a planar three-link, three-revolute-jointed manipulator mounted at the

midpoint of the axle between the two driving wheels, as depicted in Figure 2. Frame $\{M\}$ is rigidly attached to the WMR with the X_M -axis oriented in the direction of the forward travel, and Y_M -axis oriented at the direction perpendicular to X_M -axis (i.e. the direction where the WMR cannot move). Frames $\{A^k\}$, $\{B^k\}$ and $\{E^k\}$ are rigidly attached to the distal ends of first, second and third links, respectively, using the Denavit-Hartenberg convention. For generality, we will also consider that the body-fixed frame $\{E\}$ attached to the payload is offset with respect to the end-effector frame $\{E^k\}$, by a constant angle δ_k . The configuration of the manipulator with the three revolute-joints can be parameterized by the three relative angles θ_1 , θ_2 and θ_3 , with the link lengths L_1 , L_2 and L_3 .

We consider the mobile manipulator module as being composed of two subsystems (*mobile platform/manipulator*) and develop the twist-based kinematic model of each subsystem separately. The end-effector twists associated with the motion of each articulation in the subsystem are expressed in the end-effector frame $\{E\}$. The velocity kinematics for the *mobile platform* (including the effects of the nonholonomic constraints) can be written in the twist matrix form as:

$${}^M [{}^F T_M] = \begin{bmatrix} 0 & -1 & 0 \\ 1 & 0 & 0 \\ 0 & 0 & 0 \end{bmatrix} \omega_M + \begin{bmatrix} 0 & 0 & 1 \\ 0 & 0 & 0 \\ 0 & 0 & 0 \end{bmatrix} v_M \quad (7)$$

where ω_M and v_M are angular and linear forward velocities of the mobile base, respectively. These twist matrices are currently expressed in the mobile robot frame $\{M\}$. Re-expressing them in frame $\{E\}$ by similarity transformation, and extracting the components in the resulting twist matrices, the twist vectors formed are

$${}^E [{}^F t_M] = {}^E [{}^t_{\omega_M}] \omega_M + {}^E [{}^t_{v_M}] v_M \quad (8)$$

where

$${}^E [{}^t_{\omega_M}] = \begin{bmatrix} 1 \\ -L_1 \sin(\delta_k - \theta_2 - \theta_3) - L_2 \sin(\delta_k - \theta_3) - L_3 \sin \delta_k \\ L_1 \cos(\delta_k - \theta_2 - \theta_3) + L_2 \cos(\delta_k - \theta_3) + L_3 \cos \delta_k \end{bmatrix},$$

$${}^E [{}^t_{v_M}] = \begin{bmatrix} 0 \\ \cos(\delta_k - \theta_1 - \theta_2 - \theta_3) \\ \sin(\delta_k - \theta_1 - \theta_2 - \theta_3) \end{bmatrix}$$

For the *manipulator* part of the system, the total twist can be expressed as a linear combination the twist vectors of each d.o.f in the system in the form of

$${}^E [{}^F t_E] = {}^E [{}^t_{\dot{\theta}_1}] \dot{\theta}_1 + {}^E [{}^t_{\dot{\theta}_2}] \dot{\theta}_2 + {}^E [{}^t_{\dot{\theta}_3}] \dot{\theta}_3 \quad (9)$$

where

$${}^E t_{\dot{\theta}_i} = \begin{bmatrix} 1 \\ -L_1 \sin(\delta_k - \theta_2 - \theta_3) - L_2 \sin(\delta_k - \theta_3) - L_3 \sin \delta_k \\ L_1 \cos(\delta_k - \theta_2 - \theta_3) + L_2 \cos(\delta_k - \theta_3) + L_3 \cos \delta_k \end{bmatrix},$$

$${}^E t_{\dot{\theta}_2} = \begin{bmatrix} 1 \\ -L_2 \sin(\delta_k - \theta_3) - L_3 \sin \delta_k \\ L_2 \cos(\delta_k - \theta_3) + L_3 \cos \delta_k \end{bmatrix}, \quad {}^E t_{\dot{\theta}_3} = \begin{bmatrix} 1 \\ -L_3 \sin \delta_k \\ L_3 \cos \delta_k \end{bmatrix}.$$

Combining the twist vectors of both subsystems, the geometrically assembled Jacobian matrix that relate the end-effector twist and the rate of each d.o.f in the entire module can be expressed as

$${}^E [{}^F t_E] = J \underline{u} \quad (10)$$

where

$$J = \begin{bmatrix} {}^E [{}^t_{\omega_M}] & {}^E [{}^t_{v_M}] & {}^E [{}^t_{\dot{\theta}_1}] & {}^E [{}^t_{\dot{\theta}_2}] & {}^E [{}^t_{\dot{\theta}_3}] \end{bmatrix} \quad (11)$$

$$\underline{u} = [\omega_M \quad v_M \quad \dot{\theta}_1 \quad \dot{\theta}_2 \quad \dot{\theta}_3]^T \quad (12)$$

Such formulation is very useful in our system since the Jacobian matrices can be assembled modularly in different cases, which we will explore in the subsequent sections. For the remainder of the paper, we will denote the end-effector twist ${}^E t$ instead of ${}^E [{}^F t_E]$ for simplicity of notation.

V. MODELING OF COOPERATIVE PAYLOAD TRANSPORT

Multiple kinematic closed-loop constraints are formed when the common payload is placed on the end-effectors of adjacent cooperating mobile manipulator modules. In developing this model, we adopt some aspects of the formulation from [11],[34],[36]-[37]. We will treat the payload as a common reference member of Type 0 simple-closed-chain system and the various mobile manipulator modules as the serial-chain legs. For this paper, we will also assume that a rigid connection is formed between the payload and the end-effector i.e., all mobility at the contact is localized within the attaching serial-chain.

Let the complete set of joint velocities of the constrained mechanical system be described by a vector of the generalized velocities, $\underline{\eta}$. The differential-kinematic model of the closed-loop constrained system can generally be written as:

$$J_T(\underline{\eta}) \underline{\dot{\eta}} = {}^E t \quad (13)$$

subject to the general velocity-level constraint equations

$$J_C(\underline{\eta}) \underline{\dot{\eta}} = \underline{0} \quad (14)$$

We note that within a parallel-chain mechanism, not all the joints in the system need to be actuated. The mixture of active and passive joint components can help partition the rate-vector as $\underline{\eta}^T = [\underline{\eta}_a^T \quad \underline{\eta}_p^T]$. $\underline{\eta}_a$ and $\underline{\eta}_p$ are the sub-vectors of the active and passive manipulation rates variables within the entire constrained mechanical system. J_T and J_C can then be partitioned accordingly, permitting Eqs. (13) and (14) to be rewritten as:

$$J_{T_a} \underline{\dot{\eta}}_a + J_{T_p} \underline{\dot{\eta}}_p = {}^E t \quad (15)$$

$$J_{C_a} \underline{\dot{\eta}}_a + J_{C_p} \underline{\dot{\eta}}_p = \underline{0} \quad (16)$$

A general solution of Eq. (16) for $\underline{\dot{\eta}}_p$ can be determined as:

$$\underline{\dot{\eta}}_p = -J_{C_p}^+ J_{C_a} \underline{\dot{\eta}}_a + \tilde{J}_{C_p} \underline{\xi} \quad (17)$$

where the superscript $+$ denotes the Moore-Penrose inverse of the matrix, \tilde{J}_{C_p} is the right annihilator of J_{C_p} , i.e. $J_{C_p}\tilde{J}_{C_p} = \underline{0}$ and ξ is any arbitrary vector parameterizing the nullspace of J_{C_p} . Using Eq. (15) with Eq. (17), we get

$$\begin{aligned} {}^E \underline{t} &= \left[J_{T_a} - J_{T_p} J_{C_p}^+ J_{C_a} \right] \dot{\eta}_a + J_{T_p} \tilde{J}_{C_p}^+ \xi \\ &= \bar{J}_T \dot{\eta}_a + J_{T_p} \tilde{J}_{C_p}^+ \xi \end{aligned} \quad (18)$$

\bar{J}_T is the *system Jacobian matrix* which now relates the actuated joint rates of the system to the task space twists.

Actuation

Three different cases arise depending on the nature of the actuation within the system, which is reflected sizes of the matrices J_{C_a} and J_{C_p} .

Exact Actuation: If the system is exactly-actuated, as typically seen in parallel manipulators, then J_{C_p} has full rank and no longer possesses a nullspace. Thus, we can rewrite Eqs. (17) and (18) as:

$$\dot{\eta}_p = -J_{C_p}^{-1} J_{C_a} \dot{\eta}_a \quad (19)$$

$${}^E \underline{t} = \left[J_{T_a} - J_{T_p} J_{C_p}^{-1} J_{C_a} \right] \dot{\eta}_a = \bar{J}_T \dot{\eta}_a \quad (20)$$

Redundant-actuation: In a redundantly-actuated system, J_{C_p} is a rectangular $m \times n$ matrix with $m > n$ for which \tilde{J}_{C_p} does not exist and the Moore-Penrose pseudo-inverse that solves the problem in the least-squares sense, can be determined as:

$$J_{C_p}^+ = \left(J_{C_p}^T J_{C_p} \right)^{-1} J_{C_p}^T \quad (21)$$

Under-actuation: In under-actuated systems, J_{C_p} is generally a rectangular $m \times n$ matrix with $m < n$ and a non-trivial \tilde{J}_{C_p} . The existence of the $J_{T_p} \tilde{J}_{C_p}^+ \xi$ term in Eq. (18) is unique to *under-actuated closed-chain systems*. It corresponds to system *self-motion*, wherein the end-effector can still move even when all the active joints are locked. In order to prevent the self-motion, we will choose to lock a selected number of the passive joints, as determined by the size of J_{C_p} . In this case, the size of \tilde{J}_{C_p} is $n \times (n - m)$, so the dimension of the self-motion manifold is $n - m$, necessitating locking of as many passive joints in order to eliminate all system self-motion. In terms of modeling, locking the passive joints entails eliminating the column vectors the corresponding locked joints from J_{C_p} bringing us back to an exactly-actuated case.

Manipulability-based Performance Measure

The system Jacobian matrix \bar{J}_T maps the active joint rates into both the translational and orientational task-space velocities. In this paper, we will focus solely on the translational mapping – the sub-matrix of the second and the third rows of \bar{J}_T , which we denote as $\bar{J}_{T,trans}$. The singular

value decomposition (SVD) of this matrix can now be used to examine the manipulability characteristics and its interpretation in the context of the manipulability ellipsoid geometry. In our case, we adopt the *Isotropy Index* ($\Gamma_{I,trans}$) as the measure-of-choice to characterize the performance of our cooperative system.

$$\Gamma_{I,trans} = \frac{\sigma_{\min}}{\sigma_{\max}} \quad (22)$$

where σ_{\min} and σ_{\max} are the minimum and maximum singular values of the $\bar{J}_{T,trans}$. See [31],[36] for a description of some of the benefits including boundedness and excellent numerical behavior. However, $\bar{J}_{T,trans}$ depends upon the selection of the location of the actuated and unactuated joints. In subsequent sections we will examine some of the different case studies that arise due to such selection of type and location of the actuation.

VI. CASE STUDIES

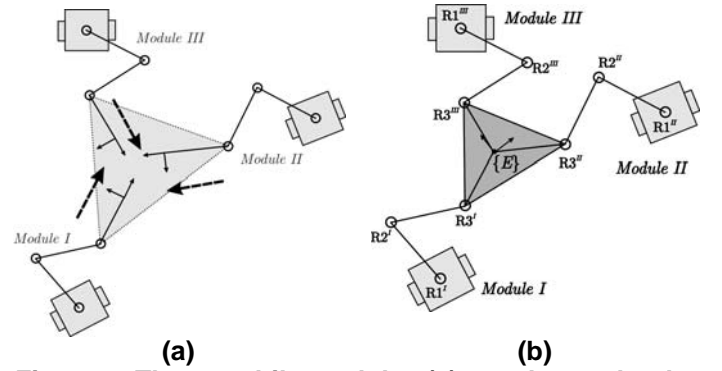


Figure 3: Three mobile modules (a) attach together by placing a common payload to effectively form (b) a composite locomotion system

We consider the case of three mobile manipulators coming together in a formation to cooperatively transport a common payload. The three-module case permits us to provide linkage to some existing literature, such as the traditional *stationary 3-RRR planar parallel mechanisms*.

The individual modules are numbered *I*, *II* and *III*, as depicted in Figure 3. We denote the revolute joints Ri^k , and the mobile bases MB^k , where $i = 1, 2, 3$ and $k = I, II, III$. When an object is placed at the end-effectors of the mobile manipulator modules, it effectively creates a *mobile 3-RRR planar parallel mechanism*. Instantaneously, each MB is considered to form a 2-d.o.f. nonholonomic joint while each revolute joint possesses 1 d.o.f. For convenience of comparison with existing literature, we will impose some further design limitations such as requiring identical mobile modules, i.e. the mobile bases have the same size and the manipulators have the same link lengths. Further, we also impose a requirement for symmetry of actuation within the contributing sub-chains.

We, however, note that the formulation can be extended to increasing numbers of modules as well as take into account the various selections of actuator locations within the system.

Twenty seven permutations are possible based on whether MB, R1 and R2 are chosen to be locked, passive or made

active. Five interesting sets of cases were identified for studied and are listed in Table 1.

Cases	MB	R1	R2
Case I	Locked	Active	Passive
Case II	Locked	Passive	Active
Case III	Active	Passive	Passive
Case IV	Active	Locked	Passive
Case V	Active	Passive	Locked

Table 1: Five candidate cases based on the actuation-status of the joints within each chain

Study Parameters

For our study, we locate the MBs at the vertices of an equilateral triangle of side $4m$, with the payload taking the form of another equilateral triangle of side $1.7321m$ as shown in Figure 4. The end-effector frame is assumed to be located at the centroid of the payload-triangle with an orientation $\phi_E = 0^\circ$. The workspace area spanned by the mechanism is very dependent on the dimensions of the links and by imposing a design criterion that $L_1^k = L_2^k$ for the modules, we can realize a symmetrical workspace, without any unreachable regions. The other critical dimensions are shown in Table 2. However, the mechanism has 8 working modes with different elbow configurations. We denote 0 and 1 for elbow up and elbow down configuration, respectively. Individual assembly mode can be identified as abc , $\forall a, b, c \in \{0, 1\}$. We will assume the elbow configuration of 111 throughout the paper. We will compute the isotropy index, bounded between 0 and 1, over the entire *feasible* workspace on a 100×100 grid with spacing of $0.004m$ and show these results in the form of surface and the contour plots.

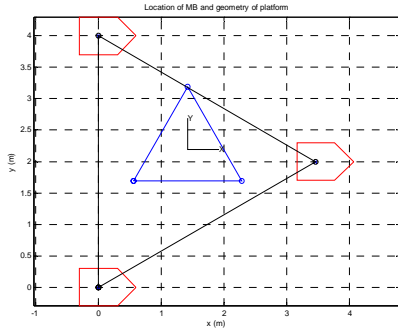


Figure 4: Location of the mobile bases and the geometry of the platform

Link Lengths	$L_1^k = 1.5m$, $L_2^k = 1.5m$, $L_3^k = 1m$
Base Positions	$(x_1^I, y_1^I) = (0, 0)$, $(x_1^{II}, y_1^{II}) = (3.4641, 2)$, $(x_1^{III}, y_1^{III}) = (0, 4)$
Platform Offset Angles	$\delta^I = 330^\circ$, $\delta^{II} = 210^\circ$, $\delta^{III} = 90^\circ$

Table 2: Detailed study parameters

Case I: MB Locked, R1 Active, R2 Passive

In this case, the mobile base of each module is locked in place and the joint R1 of each module is actuated, creating a

stationary 3-RRR^I planar parallel manipulator, as seen in Figure 5. This case was interesting from two viewpoints: First, it allows us to validate the formulation and results with existing literature [38]-[40]. Second, and more importantly, such a system results when the mobile bases are brought to a temporary halt and a relative manipulation/reconfiguration of the payload with respect to the bases is pursued.

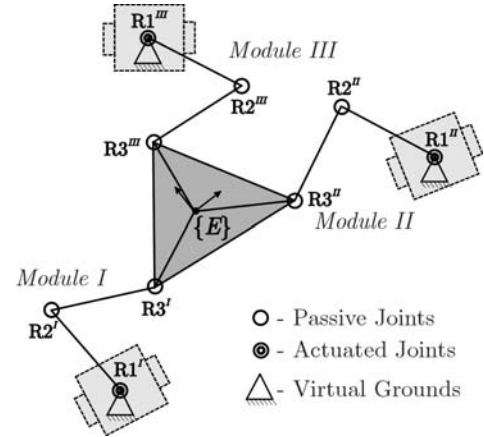


Figure 5: Case I – Cooperative system with MB Locked, R1 Active, R2 Passive

In this case, the active manipulation rates are $\dot{\eta}_a = [\dot{\theta}_1^I \ \dot{\theta}_1^{II} \ \dot{\theta}_1^{III}]^T$, and passive manipulation rates are $\dot{\eta}_p = [\dot{\theta}_2^I \ \dot{\theta}_3^I \ \dot{\theta}_2^{II} \ \dot{\theta}_3^{II} \ \dot{\theta}_2^{III} \ \dot{\theta}_3^{III}]^T$. Then,

$$J_{T_a} = \begin{bmatrix} {}^E t_{\dot{\theta}_1^I} & 0 & 0 \end{bmatrix} \quad (23)$$

$$J_{T_p} = \begin{bmatrix} {}^E t_{\dot{\theta}_2^I} & {}^E t_{\dot{\theta}_3^I} & 0 & 0 & 0 & 0 \end{bmatrix} \quad (24)$$

The system consists of two independent kinematic loop-closure constraints and these contribute 6 constraint equations. Hence, the corresponding J_{C_a} and J_{C_p} are determined as

$$J_{C_a} = \begin{bmatrix} {}^E t_{\dot{\theta}_1^I} & -{}^E t_{\dot{\theta}_1^{II}} & 0 \\ {}^E t_{\dot{\theta}_1^I} & 0 & -{}^E t_{\dot{\theta}_1^{III}} \end{bmatrix} \quad (25)$$

$$J_{C_p} = \begin{bmatrix} {}^E t_{\dot{\theta}_2^I} & {}^E t_{\dot{\theta}_3^I} & -{}^E t_{\dot{\theta}_2^{II}} & -{}^E t_{\dot{\theta}_3^{II}} & 0 & 0 \\ {}^E t_{\dot{\theta}_2^I} & {}^E t_{\dot{\theta}_3^I} & 0 & 0 & -{}^E t_{\dot{\theta}_2^{III}} & -{}^E t_{\dot{\theta}_3^{III}} \end{bmatrix} \quad (26)$$

The surface- and contour-plots of the Isotropy Index shown in Figure 6, are symmetric. The highest value occurs at the center of the workspace, which is the centroid of the triangle that the MBs formed. However, it is important to note that this surface would be different for each of the 8 kinematically distinct working modes.

¹ The underline under the first "R" indicates that the first joint of each manipulator chain is actuated.

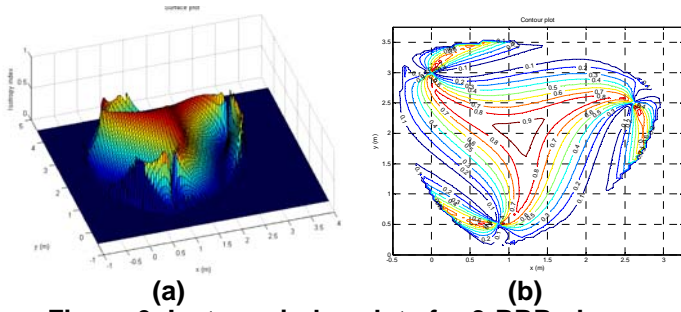


Figure 6: Isotropy index plots for 3-RRR planar parallel mechanism in Case I: (a) surface, (b) contour

Case II: MB Locked, R1 Passive, R2 Active

In this case, the mobile base of each module is again kept fixed, but we actuate R2 of each module instead of R1. This results in the stationary 3-RRR planar parallel manipulator shown in Figure 7.

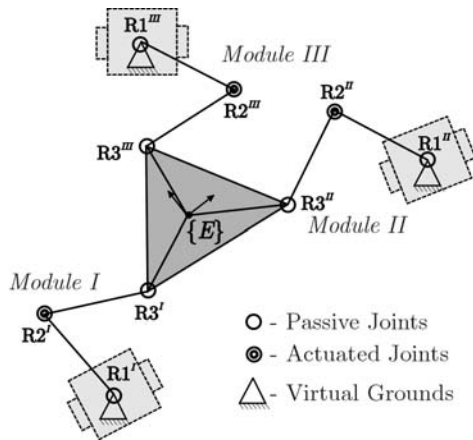


Figure 7: Case II – Cooperative system with MB Locked, R1 Passive, R2 Active

This enables us to see how the isotropy index surface changes with an alternate actuation scheme. In this case, the active manipulation rates are $\dot{\eta}_a = [\dot{\theta}_2^I \ \dot{\theta}_2^{II} \ \dot{\theta}_2^{III}]^T$, and passive manipulation rates are $\dot{\eta}_p = [\dot{\theta}_1^I \ \dot{\theta}_3^I \ \dot{\theta}_1^{II} \ \dot{\theta}_3^{II} \ \dot{\theta}_1^{III} \ \dot{\theta}_3^{III}]^T$.

Similarly, the Jacobian matrices are

$$J_{T_a} = \begin{bmatrix} {}^E t_{\phi_2}^I & \mathbf{0} & \mathbf{0} \end{bmatrix} \quad (27)$$

$$J_{T_p} = \begin{bmatrix} {}^E t_{\phi_1}^I & {}^E t_{\phi_3}^I & \mathbf{0} & \mathbf{0} & \mathbf{0} & \mathbf{0} \\ {}^E t_{\phi_1}^{II} & {}^E t_{\phi_3}^{II} & \mathbf{0} & \mathbf{0} & \mathbf{0} & \mathbf{0} \\ {}^E t_{\phi_1}^{III} & {}^E t_{\phi_3}^{III} & \mathbf{0} & \mathbf{0} & \mathbf{0} & \mathbf{0} \end{bmatrix} \quad (28)$$

$$J_{C_a} = \begin{bmatrix} {}^E t_{\phi_2}^I & -{}^E t_{\phi_2}^{II} & \mathbf{0} \\ {}^E t_{\phi_2}^I & \mathbf{0} & -{}^E t_{\phi_2}^{III} \end{bmatrix} \quad (29)$$

$$J_{C_p} = \begin{bmatrix} {}^E t_{\phi_1}^I & {}^E t_{\phi_3}^I & -{}^E t_{\phi_1}^{II} & -{}^E t_{\phi_3}^{II} & \mathbf{0} & \mathbf{0} \\ {}^E t_{\phi_1}^I & {}^E t_{\phi_3}^I & \mathbf{0} & \mathbf{0} & -{}^E t_{\phi_1}^{III} & -{}^E t_{\phi_3}^{III} \end{bmatrix} \quad (30)$$

The computed isotropy index over the feasible workspace is depicted in Figure 8. In the plots, we can see that although the geometrical (structural) properties of the mechanisms are the same with previous case, with different actuation scheme, we obtained different results. Similar to the previous case, the

workspace is symmetrical with same elbow configuration in each module and also the isotropy index surface is symmetrical. The highest value is also at the center of the workspace, which is the centroid of the triangle that the MBs formed. However, as noted in [39], the mechanism has also eight working modes, but interestingly they are all kinematically same and hence we expect the same isotropy index plots in all eight working modes.

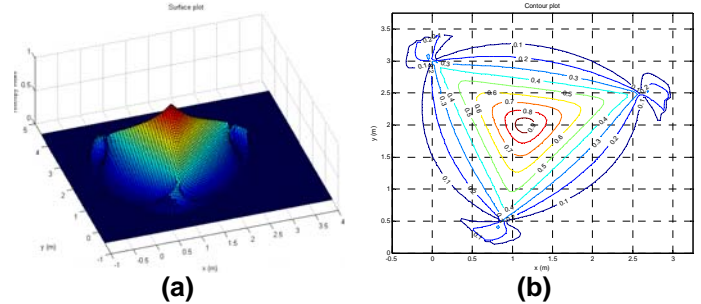


Figure 8: Isotropy index plots for 3-RRR planar parallel mechanism in Case II: (a) surface, (b) contour

Finally, we realize that both stationary 3-RRR and 3-RRR manipulators have a limited workspace. In order to span the workspace to the entire plane, we would like to make use of the mobility of the bases to create a locomotive structure.

Case III: MB Active, R1 Passive, R2 Passive

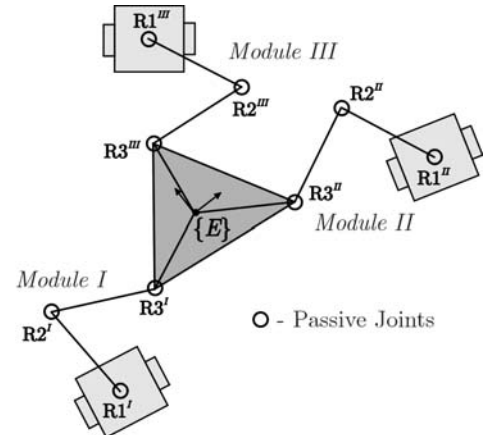


Figure 9: Case III – Cooperative system with MB Active, R1 Passive, R2 Passive

In this case, we allow the mobile base to move and free-up all the other joints within the arm as shown in Figure 9. The active-rates and passive-rates can be selected as:

$$\dot{\eta}_a = [\dot{\phi}^I \ v_M^I \ \dot{\phi}^{II} \ v_M^{II} \ \dot{\phi}^{III} \ v_M^{III}]^T,$$

$$\dot{\eta}_p = [\dot{\theta}_1^I \ \dot{\theta}_2^I \ \dot{\theta}_3^I \ \dot{\theta}_1^{II} \ \dot{\theta}_2^{II} \ \dot{\theta}_3^{II} \ \dot{\theta}_1^{III} \ \dot{\theta}_2^{III} \ \dot{\theta}_3^{III}]^T.$$

The corresponding Jacobian matrices are

$$J_{T_a} = \begin{bmatrix} {}^E t_{\phi}^I & {}^E t_{v_M}^I & \mathbf{0} & \mathbf{0} & \mathbf{0} & \mathbf{0} \end{bmatrix} \quad (31)$$

$$J_{T_p} = \begin{bmatrix} {}^E t_{\theta_1}^I & {}^E t_{\theta_2}^I & {}^E t_{\theta_3}^I & \mathbf{0} & \mathbf{0} & \mathbf{0} & \mathbf{0} & \mathbf{0} & \mathbf{0} \end{bmatrix} \quad (32)$$

Although the mobile bases can move, we consider them instantaneously located at the positions noted in the study

parameters. So, there are still 6 independent constraint equations and the corresponding J_{C_a} and J_{C_p} are:

$$J_{C_a} = \begin{bmatrix} E t_{\phi}^I & E t_{\phi}^I & -E t_{\phi}^{II} & -E t_{\phi}^{II} & 0 & 0 \\ E t_{\phi}^I & E t_{\phi}^I & 0 & 0 & -E t_{\phi}^{III} & -E t_{\phi}^{III} \end{bmatrix} \quad (33)$$

$$J_{C_p} = \begin{bmatrix} E t_{\phi_1}^I & E t_{\phi_2}^I & E t_{\phi_3}^I & -E t_{\phi_1}^{II} & -E t_{\phi_2}^{II} & -E t_{\phi_3}^{II} & 0 & 0 & 0 \\ E t_{\phi_1}^I & E t_{\phi_2}^I & E t_{\phi_3}^I & 0 & 0 & 0 & -E t_{\phi_1}^{III} & -E t_{\phi_2}^{III} & -E t_{\phi_3}^{III} \end{bmatrix} \quad (34)$$

In this case, J_{C_p} is 6×9 , so this system is *under-constrained*. Hence, we need to lock $9 - 6 = 3$ joints in the system in order to eliminate all self-motion, which leads us to explore these last two cases.

Case IV: MB Active, R1 Locked, R2 Passive

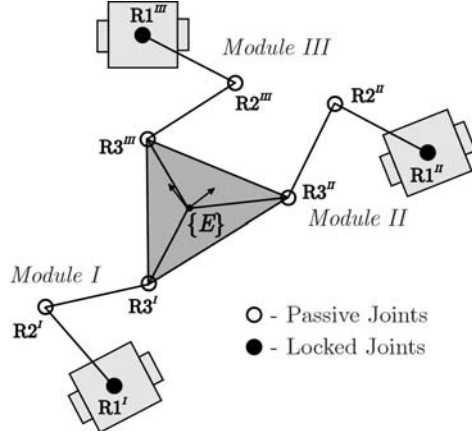


Figure 10: Case IV – Cooperative system with MB Active, R1 Locked, R2 Passive

Referring to Figure 10, the active manipulation rates are $\dot{\underline{q}}_a = [\dot{\phi}^I \ v_M^I \ \dot{\phi}^{II} \ v_M^{II} \ \dot{\phi}^{III} \ v_M^{III}]^T$, and passive manipulation rates are $\dot{\underline{q}}_p = [\dot{\theta}_2^I \ \dot{\theta}_3^I \ \dot{\theta}_2^{II} \ \dot{\theta}_3^{II} \ \dot{\theta}_2^{III} \ \dot{\theta}_3^{III}]^T$.

The corresponding Jacobian matrices are

$$J_{T_a} = \begin{bmatrix} E t_{\phi}^I & E t_{v_M}^I & 0 & 0 & 0 & 0 \\ E t_{\phi}^I & E t_{v_M}^I & 0 & 0 & 0 & 0 \end{bmatrix} \quad (35)$$

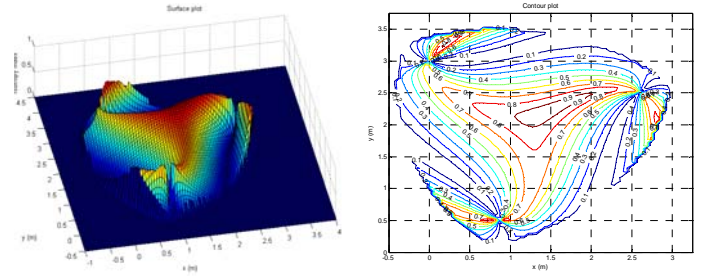
$$J_{T_p} = \begin{bmatrix} E t_{\theta_2}^I & E t_{\theta_3}^I & 0 & 0 & 0 & 0 \\ E t_{\theta_2}^I & E t_{\theta_3}^I & 0 & 0 & 0 & 0 \end{bmatrix} \quad (36)$$

$$J_{C_a} = \begin{bmatrix} E t_{\phi}^I & E t_{\phi}^I & -E t_{\phi}^{II} & -E t_{\phi}^{II} & 0 & 0 \\ E t_{\phi}^I & E t_{\phi}^I & 0 & 0 & -E t_{\phi}^{III} & -E t_{\phi}^{III} \end{bmatrix} \quad (37)$$

$$J_{C_p} = \begin{bmatrix} E t_{\theta_2}^I & E t_{\theta_3}^I & -E t_{\theta_2}^{II} & -E t_{\theta_3}^{II} & 0 & 0 \\ E t_{\theta_2}^I & E t_{\theta_3}^I & 0 & 0 & -E t_{\theta_2}^{III} & -E t_{\theta_3}^{III} \end{bmatrix} \quad (38)$$

As noted earlier, the MBs are instantaneously located at their current positions but are actuated. Hence they contribute to the overall manipulability of the platform as can be seen from the isotropy index plots, shown in Figure 11.

In the plots, we note that due to the nonholonomic constraints imposed on the MBs, the isotropy index surface plot is no longer symmetrical (in contrast to Case I). Further, the configuration for which the isotropy index is maximum is no longer at the centroid of the triangle formed by the location of the MBs.



(a) (b)
Figure 11: Isotropy index plots for the *mobile planar 3-RRR parallel mechanism with R1 locked in Case IV:* (a) surface and (b) contour plots

Case V: MB Active, R1 Passive, R2 Locked

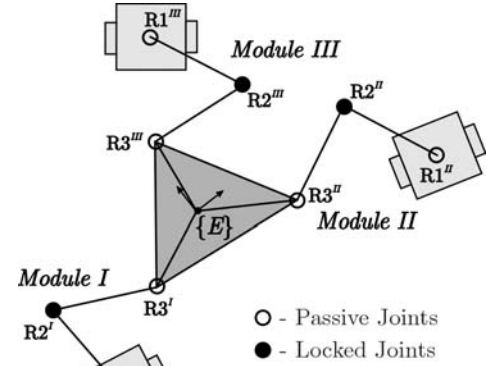


Figure 12: Case V – Cooperative system with MB Active, R1 Passive, R2 Locked

In this case, we would like to see the effect on the manipulability when locking different joints in the system. Referring to Figure 12, we allow the MBs to move but lock the joints R2 in each module. The active manipulation rates are

$\dot{\underline{q}}_a = [\dot{\phi}^I \ v_M^I \ \dot{\phi}^{II} \ v_M^{II} \ \dot{\phi}^{III} \ v_M^{III}]^T$ and passive manipulation rates are $\dot{\underline{q}}_p = [\dot{\theta}_1^I \ \dot{\theta}_3^I \ \dot{\theta}_1^{II} \ \dot{\theta}_3^{II} \ \dot{\theta}_1^{III} \ \dot{\theta}_3^{III}]^T$.

The corresponding Jacobian matrices are

$$J_{T_a} = \begin{bmatrix} E t_{\phi}^I & E t_{v_M}^I & 0 & 0 & 0 & 0 \\ E t_{\phi}^I & E t_{v_M}^I & 0 & 0 & 0 & 0 \end{bmatrix} \quad (39)$$

$$J_{T_p} = \begin{bmatrix} E t_{\theta_1}^I & E t_{\theta_3}^I & 0 & 0 & 0 & 0 \\ E t_{\theta_1}^I & E t_{\theta_3}^I & 0 & 0 & 0 & 0 \end{bmatrix} \quad (40)$$

$$J_{C_a} = \begin{bmatrix} E t_{\phi}^I & E t_{\phi}^I & -E t_{\phi}^{II} & -E t_{\phi}^{II} & 0 & 0 \\ E t_{\phi}^I & E t_{\phi}^I & 0 & 0 & -E t_{\phi}^{III} & -E t_{\phi}^{III} \end{bmatrix} \quad (41)$$

$$J_{C_p} = \begin{bmatrix} E t_{\theta_1}^I & E t_{\theta_3}^I & -E t_{\theta_1}^{II} & -E t_{\theta_3}^{II} & 0 & 0 \\ E t_{\theta_1}^I & E t_{\theta_3}^I & 0 & 0 & -E t_{\theta_1}^{III} & -E t_{\theta_3}^{III} \end{bmatrix} \quad (42)$$

The plots of the isotropy index are shown in Figure 13. In the plots, we see that locking different joints changes the manipulability characteristic in contrast with Cases IV (and with the Case II discussed earlier).

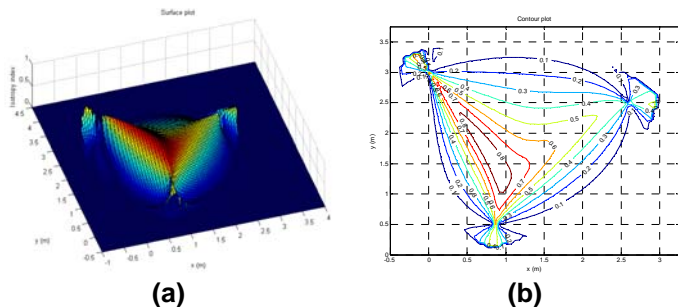


Figure 13: Isotropy index plots for the mobile 3-RRR parallel mechanism with R2 locked in Case V: (a) surface and (b) contour plots

VII. DISCUSSION AND CONCLUSION

In this paper, we examined the formulation of the system-level Isotropy Index of the entire cooperating system as a measure of overall system performance for different actuation schemes. In particular, we treated the cooperating system as a Type 0 simple constrained mechanical system. In our work, we leverage the development from the literature on constrained mechanical systems to create unified kinematic model of the overall system. This framework takes the nonholonomic constraints, kinematic loop-closure constraints and mixtures of active, locked and passive joints into account explicitly.

System-level performance measures are developed for the overall cooperating system, in terms of the system-level Jacobian matrix. In this paper, we recognize that the cooperating system performance depends critically upon the dimension, configuration and actuation and focused on the role of the joint-actuation-schemes within the system. The designer has the capability of selectively actuating, locking or rendering passive the various joints within the system – all of which affect the system performance. The case studies, using the mobile 3-RRR planar manipulator configuration permitted us to study the effect of different actuation schema on the isotropy index surface.

High values of the isotropy-index at a point or over a region of the configuration-space of the system indicate the payload is *equally manipulable* in every direction in the plane. Early efforts at creating optimization-based methods of determining an *optimal set of system-configurations* which retain high values of the isotropy index is reported in [41].

ACKNOWLEDGMENTS

We gratefully acknowledge the support from The Research Foundation of State University of New York and National Science Foundation CAREER Award (IIS-0347653) for this research effort. We also gratefully acknowledge Rajankumar Bhatt for his valuable comments and numerous suggestions.

REFERENCES

[1] Adams, J., Bajcsy, R., Kosecka, J., Kumar, V., Mandelbaum, R., Mintz, M., Paul, R., Wang, C. C., Yamamoto, Y., and Yun, X., 1995, "Cooperative Material Handling by Human and Robotic Agents: Module Development and System Synthesis," *Proc. 1995 IEEE/RSJ International Conference on Intelligent Robotics and Systems*.

[2] Abou-Samah, M., 2001, "A Kinematically Compatible Framework for Collaboration of Multiple Nonholonomic

Wheeled Mobile Robots," M.S. thesis, Mechanical Engineering, McGill University, Montreal, Quebec.

[3] Bhatt, R. M., 2004, "Formation Motion Planning for Payload Transport by Modular Wheeled Mobile Manipulators," M.S. thesis, Department of Mechanical and Aerospace Engineering, University at Buffalo.

[4] Arkin, R. C., and Bekey, G. A. (Eds.), 1997, *Robot Colonies*, Special Issue of *Autonomous Robots*, **4**(5), reprinted by Kluwer Academic Publishers, Boston.

[5] Cao, Y., Fukunaga, A. S., and Kahng, A. B., 1997, "Cooperative Mobile Robotics: Antecedents and Directions," *Autonomous Robots*, **4**(1), pp. 7-27.

[6] Koivo, A. J. and Bekey, G. A., 1988, "Report of Workshop on Coordinated Multiple Robot Manipulators: Planning, Control, and Application," *IEEE Transactions on Robotics and Automation*, **4**, pp. 91-93.

[7] Kerr, J. and Roth, B., 1986, "Analysis of Multifingered Hands," *The International Journal of Robotics Research*, **4**(4), pp. 3-17.

[8] Salisbury, J. K., and Craig, J. J., 1982, "Articulated Hands: Force Control and Kinematic Issues," *The International Journal of Robotics Research*, **1**(1), pp. 4-17.

[9] Kumar, V. and Waldron, K.J., 1988, "Force Distribution in Closed Kinematic Chains," *IEEE Transactions on Robotics and Automation*, **4**(6), pp. 657-64.

[10] Song, S. M., and Waldron, K. J., 1989, *Machines that Walk*, MIT Press, Cambridge MA.

[11] Lilly, K.W., 1993, *Efficient dynamic simulation of robotic mechanisms*, Kluwer.

[12] Khatib, O., Yokoi, K., Chang, K., Ruspini, D., Holmberg, R., and Casal, A., 1996, "Vehicle/arm Coordination and Multiple Mobile Manipulator Decentralized Cooperation," *Proc. 1996 IEEE/RSJ International Conference on Intelligent Robots & Systems '96, IROS 96*, Vol.2, pp. 546 – 553.

[13] Desai, J. and Kumar, V., 1999, "Motion Planning for Cooperating Mobile Manipulators," *Journal of Robotic Systems*, **10**, pp. 557-579

[14] Tanner, H. G., Kyriakopoulos, K. J., and Krikelis, N. I., 1998, "Modeling of Multiple Mobile Manipulators Handling a Common Deformable Object," *Journal of Robotic Systems* **15**(11), pp. 599-623.

[15] Kosuge, K., Oosumi, T., Sato, M., Chiba, K., and Takeo, K., 1998, "Transportation of a Single Object by Two Decentralized-controlled Nonholonomic Mobile Robots", *Proc. 1998 IEEE International Conference on Intelligent Robots and Systems*, pp.2989-2994.

[16] Yamakita, M. and Suh, J-H., 2001, "Adaptive Generation of Desired Velocity Field for Leader-Follower Type Cooperative Mobile Robots with Decentralized PVFC," *Proc. 2001 IEEE International Conference on Robotics and Automation*, vol.4, pp. 3495 –3502.

[17] Krishnaprasad, P.S., and Tsakiris, D.P., 1995, "Oscillations, SE(2)-Snakes and Motion Control" *34rd IEEE Conference on Decision and Control*, New Orleans, LA, pp. 2806-11.

- [18] Ostrowski, J.P., 1995, "The Mechanics and Control of Undulatory Robotic Locomotion," Ph. D. thesis, California Institute of Technology, Pasadena, CA.
- [19] Borenstein, J., Everett, B., and Feng, L., 1996, *Navigating Mobile Robots: Systems and Techniques*, A. K. Peters, Ltd., Wellesley, MA.
- [20] Campion, G., Bastin, G., and D'Andrea-Novell, B., 1996, "Structural Properties and Classification of Kinematic and Dynamic Models of Wheeled Mobile Robots," *IEEE Transactions on Robotics and Automation*, **12**(1), pp.47-62.
- [21] Pin, F. G. and Killough, M., 1994, "A New Family of Omnidirectional and Holonomic Wheeled Platforms for Mobile Robots," *IEEE Transactions on Robotics and Automation*, **10**(4), pp.480-489.
- [22] Reister, D.B. and Unseren, M.A., 1993, "Position and Constraint Force Control of a Vehicle with Two or More Steerable Drive Wheels," *IEEE Transactions on Robotics and Automation*, **9**(6), pp.723-731.
- [23] Sreenivasan S.V., and Waldron K. J., 1996, "Displacement Analysis of an Actively Articulated Wheeled Vehicle Configuration with Extensions to Motion Planning on Uneven Terrain," *ASME Journal of Mechanical Design*, **118**(2), pp. 312-317.
- [24] Nakamura, Y., 1991, *Advanced Robotics: Redundancy and Optimization*, Addison-Wiley Publishing Company.
- [25] Balch, T., 2000, "Hierarchic Social Entropy: An Information Theoretic Measure of Robot Group Diversity," in *Autonomous Robots 8*, Kluwer Academic Publishers, Netherlands, pp. 209-237.
- [26] Bhatt, R. M., Tang, C. P., and Krovi, V., 2004, "Geometric Motion Planning and Formation Optimization for a Fleet of Nonholonomic Wheeled Mobile Robots," in *Proc. 2004 IEEE International Conference of Robotics and Automation*, New Orleans, LA.
- [27] Belta, C. and Kumar, V., 2004, "Optimal Motion Generation for Groups of Robots: A Geometric Approach," *ASME Journal of Mechanical Design*, **126**(1), pp. 63-70.
- [28] Zefran, M., Kumar, V., and Croke, C. B., 1998, "On the Generation of Smooth Three-dimensional Rigid Body Motions," *IEEE Transactions on Robotics and Automation*, **14**(4), pp. 576-589.
- [29] Yoshikawa, T., 1985, "Manipulability of Robotic Mechanisms," *The International Journal of Robotics Research*, **4**(2), pp. 3-9.
- [30] Yamamoto, Y., and Yun, X., 1994, "Coordinating Locomotion and Manipulation of a Mobile Manipulator," *IEEE Transactions on Automatic Control*, **39**(6), pp. 1326-1332.
- [31] Zanganeh, K. E., and Angeles, J., 1997, "Kinematic Isotropy and the Optimum Design of Parallel Manipulators," *International Journal of Robotic Research*, **16**(2), pp. 185-197.
- [32] Bicchi, A., and Prattichizzo, D., 2000, "Manipulability of Cooperating Robots with Unactuated Joints and Closed-chain Mechanisms," *IEEE Transactions on Robotics and Automation*, **16**(4), pp. 336-345.
- [33] Park, F. C., and Kim, J. W., 1998, "Manipulability and Singularity Analysis of Multiple Robot Systems: A Geometric Approach," *Proc. 1998 IEEE International Conference on Robotics and Automation*, Leuven, Belgium.
- [34] Wen, J. T.-Y., and Wilfinger, L. S., 1999, "Kinematic Manipulability of General Constrained Rigid Multibody Systems," *IEEE Transactions on Robotics and Automation*, **15**(3), pp. 558-567.
- [35] Murray, R.M., Li, Z., and Sastry, S.S., 1994, *A Mathematical Introduction to Robotics Manipulation*, CRC Press, London, UK.
- [36] Angeles, J., 2003, *Fundamental of Robotics Mechanical Systems – Theory, Methods, and Algorithms*, 2nd Ed., Springer-Verlag New York, Inc., New York.
- [37] Tsai, L.-W., 1999, *Robot Analysis: The Mechanics of Serial and Parallel Manipulators*, John Wiley & Sons, New York, NY.
- [38] Ma, O., and Angeles, J., 1989, "Direct Kinematics and Dynamics of a Planar 3-dof Parallel Manipulator," *Advances in Design Automation*, ASME Montreal, Quebec, **3**, pp. 313-320.
- [39] Bonev, I.A., 2002, "Geometric Analysis of Parallel Mechanisms," Ph. D. thesis, Department of Mechanical Engineering, Laval University, Quebec City, QC Canada.
- [40] Chan, V.K. and Ebert-Uphoff, I., 2001, "Investigation of the Deficiencies of Parallel Manipulators in Singular Configurations through the Jacobian Nullspace," *Proc. 2001 IEEE International Conference on Robotics and Automation*, Seoul, Korea.
- [41] Tang, C. P., 2004, "Manipulability-Based Analysis of Cooperative Payload Transport by Robot Collectives," M.S. thesis, Department of Mechanical & Aerospace Engineering, State University of New York at Buffalo, Buffalo, NY.